A novel near-infrared fluorescent and colorimetric probe for selective detection of Ag^{+} and Hg^{2+}

Min, Yuquan; Han, Xin; Qi, Youguo; Jiang, Lin; Song, Yanxi; Ma, Yilin; Zhang, Jian; Li, Hongqi

Published in:
Coloration Technology

Link to article, DOI:
10.1111/cote.12687

Publication date:
2024

Document Version
Peer reviewed version

A novel near-infrared fluorescent and colorimetric probe for selective detection of Ag^+ and Hg^{2+}

Yuquan Min[a], Xin Han[b,*], Youguo Qi[a], Lin Jiang[a], Yanxi Song[c], Yilin Ma[a], Jian Zhang[a], Hongqi Li[a,*]

[a]*College of Chemistry and Chemical Engineering, Donghua University, Shanghai 201620, China*

[b]*Department of Health Technology, Technical University of Denmark, Kongens Lyngby, 2800, Denmark*

[c]*College of Environmental Science and Engineering, Donghua University, Shanghai 201620, China*

E-mail: sssshanxin@gmail.com; hongqili@dhu.edu.cn

Received:

ABSTRACT

It is particularly important to develop effective and specific detection methods for harmful metal ions Ag^+ and Hg^{2+} sensing. In this paper, a new near infrared (NIR) fluorescent probe **N-FP** based on intramolecular charge transfer (ICT) effect was designed and synthesized, which exhibited the characteristics of large Stokes shift (163 nm) and excellent stability. Addition of Ag^+ or Hg^{2+} to probe **N-FP** solution in EtOH/H_2O (9:1, v/v) caused remarkable enhancement of fluorescence emission at 661 nm, bathochromic shift of UV-vis absorption wavelength, and color change from orange to red or purple. While adding other metal ions including Li^+, Na^+, K^+, Ag^+, Cu^{2+}, Fe^{2+}, Zn^{2+}, Co^{2+}, Ni^{2+}, Mn^{2+}, Sr^{2+}, Ca^{2+}, Mg^{2+}, Al^{3+}, Cr^{3+} and Fe^{3+} did not bring about substantial spectral and color change. The detection limit of probe **N-FP** for Ag^+ and Hg^{2+} was calculated to be 1.1 μM and 0.72 μM, respectively. Probe **N-FP** could be used to recognition Ag^+ and Hg^{2+} in a wide pH range of 1-10. The sensing mechanism was proposed and demonstrated by ^1H NMR, HPLC and MS measurements.

Keywords: Near infrared; Fluorescence probe; Stokes shift; Ag^+; Hg^{2+}

1. Introduction

Nowadays people are more and more concerning of the use and impacts of heavy metals. Among them Hg^{2+} and Ag^+ ions have been designated as typical hazards as they can cause permanent adverse effects on human organs like liver, kidney, lung, and nervous system [1]. In view of the harm of Hg^{2+} and Ag^+ ions to the environment

This article has been accepted for publication and undergone full peer review but has not been through the copyediting, typesetting, pagination and proofreading process which may lead to differences between this version and the Version of Record. Please cite this article as doi: 10.1111/cote.12687

and human body, it is particularly necessary to develop effective analytical methods for Hg^{2+} and Ag^{+} detection. Many analytical methods include atomic absorption spectrometry [2,3], plasma atomic emission spectrometry [4], and atomic fluorescence spectrometry [5] have been applied for determination of Hg^{2+} and Ag^{+}. However, these methods are too complicated and time-consuming and vulnerable to other factors. In contrast, fluorescent probe detection has attracted much attention due to its rapidity and convenience, short response time, high sensitivity and strong anti-interference ability and over the past years numerous fluorescent probes have been developed for detection of Hg^{2+} and Ag^{+} [6–13]. Multifunctional fluorogenic chemosensors for simultaneous or discriminative detection of Hg^{2+} and Ag^{+} have also been reported based on metal-organic frameworks (MOFs) [14–16], polymers [17–19], DNA [20,21], quantum dots [22–24], carbon dots [24,25], gold nanoclusters [26,27], nanoparticles [28,29], nanoribbons [30], fluorescent silk [31], chromatography paper [32], and small organic molecules such as 1,8-naphthalimides [33–35], calix[4]arenes [36,37], BODIPY derivatives [38], thienyldiketopyrrolopyrrole [39], 9,9'-bianthracene [40], 1,8-naphthyridine derivatives [41], 7-nitrobenzo-2-oxa-1,3-diazolyl (NBD) [42], rhodamine B [43], fluorescein derivatives [44], coumarins [45], triarylamine rhodanine derivatives [46], chromene-imidazophenazine [47], and pyridyl azo compounds [48].

However, these reported probes generally exhibited poor selectivity due to the serious interference from Cu^{2+} [24,29,37,49,50], Pb^{2+} [20,23,51,52], F^{-} [39,41,53], Ni^{2+} [15], ClO^{-} [17], or carbonate [54]. Moreover, the Stokes shifts of these probes are small and their emission wavelengths are short and do not reach near infrared (NIR) region. Recently, on purpose of eliminating autofluorescence, improving signal/noise ratio, and increasing tissue penetration depth, we developed a new NIR spectroscopic probe for simultaneous sensing of Hg^{2+} and Ag^{+}, which displayed an extremely large Stokes shift and excellent pH adaptability and was successfully applied to in vitro U87MG cell imaging [55]. Nevertheless, the chemosensor based on coumarin-dicyanoisophorone dyad suffers from multistep synthesis. In order to obtain novel NIR fluorescent probes that are structurally simple and can be facilely synthesized, we abandon the coumarin moiety and resort to the dicyanoisophorone fluorophore because its derivatives constitute a reservoir of NIR sensors with simple structures by straightforward modification of dicyanoisophorone [56–63]. In this paper we envisage to design and synthesize a fluorescently activated NIR probe for the detection of Ag^{+}/Hg^{2+} based on intramolecular charge transfer (ICT) effect, by

condensation of 4-diethylamino salicylaldehyde with dicyanoisophorone and subsequent esterification with phenyl chlorothionocarbonate. Dicyanoisophorone as strong electron-withdrawing group and diethylamino as electron donor were introduced into the probe **N-FP** to achieve large Stokes shift, strong luminescence and ICT effect, and the emission wavelength in NIR region. The phenyl thionocarbonate moiety serves the recognition site and when Ag^{+}/Hg^{2+} is added the probe **N-FP** can be hydrolyzed to induce remarkable fluorescence enhancement and color change [64]. Owing to the ICT effect, this fluorophore exhibits long-wavelength red emission. These characteristics enable the probe to have a large Stokes shift, good selectivity, and low detection limits. It also has superb pH adaptablity and thereby good application prospect in complex environments.

2. Experimental section

2.1 Materials and equipments

All chemicals used in the experiment including isophorone, malononitrile, triethylamine, dichloromethane, piperidine, 4-(diethylamino)-2-hydroxybenzaldehyde, phenyl chlorothionocarbonate, ethanol, and metal salts are purchased from common commercial sources, unless otherwise indicated, no purification is required prior to direct use.

Nuclear magnetic resonance (NMR) spectra were recorded on a Bruker AM-400 spectrometer. Mass spectrum was measured on an Agilent LC-MS 6120 spectrometer. UV-vis absorption spectra were measured by using a Shimadzu UV-3600 Plus UV-visible and near infrared spectrophotometer. Fluorescence emission spectra were obtained on a Hitachi F 7000 fluorescence spectrophotometer.

*2.2 Synthesis of compound **N-OH***

Compound **1** was synthesized according to known procedure reported in literature, mp: 70–71 °C (literature value: 70.2–72.6 °C [65]). Compound **1** (558 mg, 3.0 mmol) and 4-(diethylamino)-2-hydroxybenzaldehyde (579 mg, 3.0 mmol) were dissolved in 25 mL of anhydrous ethanol. Then 0.3 mL of piperidine was added and the mixture was heated to 80 °C with stirring for 7 h. After reaction the solvent was removed in vacuum. Purple red solid of **N-OH** was obtained by silica gel column chromatography

in 74% yield with petroleum ether/ethyl acetate (6:1, v/v) as eluent, mp: 160.1–161.4 ℃. IR (KBr pellet): ν 3333, 2961, 2923, 2219, 1526, 1490, 1129, 1073 cm^{-1}.

*2.3 Synthesis of probe **N-FP***

Compound **N-OH** (722 mg, 2.0 mmol) and phenyl chlorothionocarbonate (413 mg, 2.4 mmol) were mixed and dissolved in dichlooromethane (DCM, 15 mL). Triethylamine (0.34 mL, 202 mg, 2.0 mmol) was added and the mixture was stirred at 0 °C overnight. Thin layer chromatography was used to monitor the reaction with petroleum ether/ethyl acetate (8:1, v/v) as developer. After the reaction was completed water was added for quenching. The organic layer was extracted with DCM and dried with anhydrous magnesium sulfate. Black solid of **N-FP** was obtained after purification with silica gel column chromatography with petroleum ether/ethyl acetate (15:1, v/v) as eluent. Yield: 646 mg (65%), mp: 140.5–142.6℃. The purity of **N-FP** was 99.08% measured by HPLC under conditions: column dimensions 150 mm × 4.6 mm × 5 μm, WondaSil-C18 as the stationary phase, acetonitrile/water (9:1, v/v) as the mobile phase: detection wavelength 498 nm, flow rate 2 mL min^{-1}, temperature 30℃. IR (KBr pellet): ν 3068, 2957, 2213, 1547, 1501, 1206, 1154 cm^{-1}. ^{1}H NMR (400 MHz, DMSO-d_6) δ 7.79–7.76 (m, 1H), 7.57–7.49 (m, 2H), 7.40–7.36 (m, 1H), 7.31–7.29 (m, 2H), 7.17–7.04 (m, 2H), 6.78 (s, 1H), 6.70 (dd, J = 9.0, 2.7 Hz, 1H), 6.62 (d, J = 2.6 Hz, 1H), 3.42 (q, J = 7.0 Hz, 4H), 2.61 (s, 2H), 2.53 (s, 2H), 1.12 (t, J = 7.0 Hz, 6H), 1.04 (s, 6H). ^{13}C NMR (101 MHz, DMSO-d_6) δ 193.91, 170.38, 156.87, 153.72, 153.58, 150.33, 131.27, 129.71, 127.58, 126.18, 122.10, 121.64, 114.76, 114.57, 113.96, 111.00, 105.11, 74.72, 44.53, 42.74, 38.63, 32.09, 27.94, 12.98. LR-MS: m/z 498 $(M+1)^{+}$. HR-MS: m/z 497.2113; calcd. for $C_{30}H_{31}N_3O_2S$ 497.2137.

2.4 Measurement of absorption and fluorescence spectra

Probe **N-FP** was dissolved in solvents to prepare the stock solution (20 μM) for spectral measurements. The required metal ion stock solution (20 μM) was prepared before fluorescence and UV-vis spectral tests by dissolving the salts LiCl, $NaNO_3$, KNO_3, $AgNO_3$, $Cu(NO_3)_2$, $Fe(SO_4)_2{\cdot}7H_2O$, $Zn(NO_3)_2$, $CoCl_2{\cdot}6H_2O$, $NiCl_2{\cdot}6H_2O$, $Mn(NO_3)_2{\cdot}4H_2O$, $SrCl_2$, $Hg(OAc)_2$, $CaCl_2$, $Mg(NO_3)_2$, $Al(NO_3)_3{\cdot}9H_2O$, $Cr(NO_3)_3$ and $Fe(NO_3)_3{\cdot}9H_2O$ in deionized water. UV-vis absorption and fluorescence emission measurements were performed at around 25 °C. The excitation wavelength was 498

nm for fluorescence spectral test with both the excitation and emission slits being 5.0 nm.

3. Results and discussion

*3.1 Synthesis and structural characterization of probe **N-FP***

The target probe **N-FP** was synthesized by a three step protocol, as showed in Fig. 1. Compund **1** was prepared by a simple condensation reaction between malononitrile and isophorone and was used to react with 4-(diethylamino)-2-hydroxybenzaldehyde catalyzed with piperidine in anhydrous alcohol. The Knoevenagel reaction generated a bright NIR fluorophore **N-OH** in 74% yield and its structure was confirmed by FTIR spectrum (Fig. S1) [66]. Thiocarbonate acceptor part of Hg^{2+}/Ag^{+} has a strong affinity so was selected as the recognition group. In the third step, the probe **N-FP** was prepared by the reaction of **N-OH** with phenyl chlorothiocarbonate under the condition of acid reagent. The chemical structure of the target probe **N-FP** was confirmed by ^{1}H NMR (Fig. S2), ^{13}C NMR (Fig. S3), mass spectrum (Fig. S4), and FTIR spectrum (Fig. S5). All the spectral data were in good accordance with the target structure. The purity of probe **N-FP** was determined to be 99.08% by HPLC (Fig. S6 and Table S1).

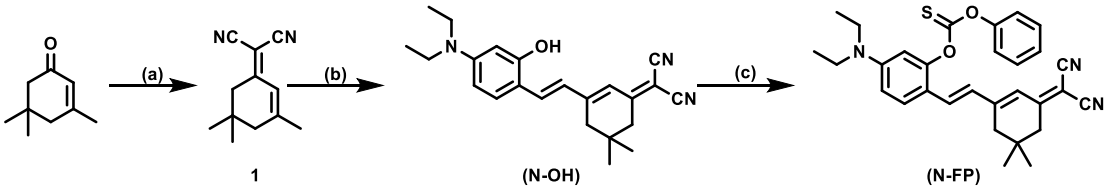

Fig. 1. Synthetic route of probe **N-FP**. Reaction conditions: (a) malononitrile, anhydrous ethanol, piperidine, argon atmosphere, refluxed at 80 °C for 13 h. (b) 4-(diethylamino)-2-hydroxybenzaldehyde, anhydrous ethanol, piperidine, refluxed at 80 ℃ for 6 h. (c) phenyl chlorothionocarbonate, dry DCM, piperidine, stirred at 0 ℃ for 6 h.

*3.2 Fluorescence emission spectra of probe **N-FP** in different solvents*

Fluorescence spectra of probe **N-FP** (20 μM) in different solvents including methanol (MeOH), ethanol (EtOH), DCM, ethyl acetate (EA), acetonitrile (CH_3CN), DMSO and dimethylformamide (DMF) were measured and showed in Fig. 2 (a). It could be

observed that the maximum absorption wavelength and the fluorescence intensity of probe **N-FP** varied in different solvents. Ethanol was selected as the test solvent because probe **N-FP** exhibited relatively strong fluorescence in ethanol and distinct color change after addition of Ag^{+} and Hg^{2+} in ethanol. Though the fluorescence intensities of probe **N-FP** in DMSO and DMF were much stronger than that in ethanol, the color change of probe **N-FP** solution upon addition of Ag^{+} and Hg^{2+} in DMSO or DMF was not sufficiently obvious. To ascertain whether probe **N-FP** was applicable in aqueous solutions, fluorescence spectra of probe **N-FP** (20 μM) in EtOH/H_2O of different ratio (10:0, 9:1, 8:2, 7:3, 6:4, 5:5, 4:6, 3:7, 2:8, 1:9, 0:10, v/v) were measured and showed in Fig. 2 (b). With the increase of water content in the solvent, the fluorescence intensity of probe **N-FP** decreased significantly. When the water content was more than 50%, the fluorescence was almost quenched. So EtOH/H_2O (9:1, v/v) was chosen as the medium for subsequent detection tests based on the results.

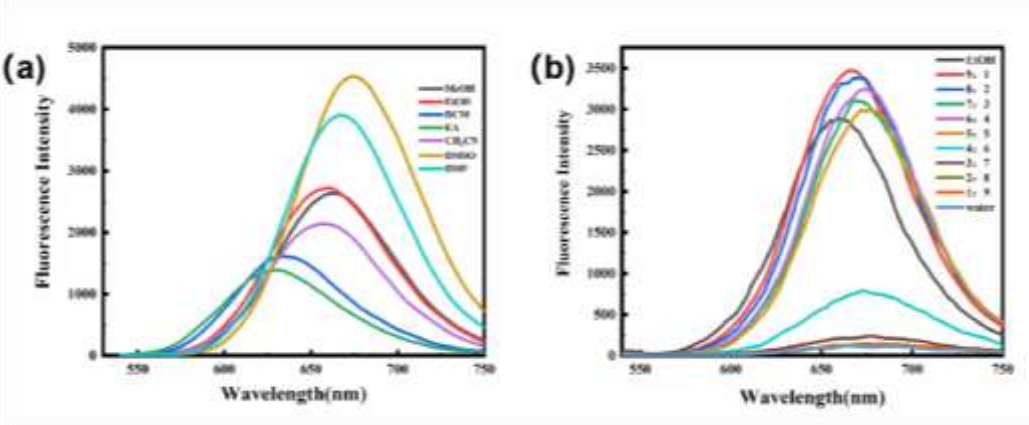

Fig. 2. Fluorescence spectra of probe **N-FP** (20 μM) in different solvents (a) and in EtOH/H_2O of different ratio (10:0, 9:1, 8:2, 7:3, 6:4, 5:5, 4:6, 3:7, 2:8, 1:9, 0:10, v/v) (b) with excitation wavelength of 498 nm.

*3.3 Selectivity of probe **N-FP** for detection of Ag^{+} and Hg^{2+}*

Color of the solution of probe **N-FP** in EtOH/H_2O (9:1, v/v) turned out to be orange. Addition of Ag^{+} and Hg^{2+} to the solution caused the color change from orange to red and purple, respectively. While adding other metal ions including Li^{+}, Na^{+}, K^{+}, Cu^{2+}, Fe^{2+}, Zn^{2+}, Co^{2+}, Ni^{2+}, Mn^{2+}, Sr^{2+}, Ca^{2+}, Mg^{2+}, Al^{3+}, Cr^{3+} and Fe^{3+} failed to bring about obvious color change, as showed in Fig. 3. Therefore, probe **N-FP** can be used for naked eye detection of Ag^{+} and Hg^{2+}. The maximum absorption wavelength of probe **N-FP** in EtOH/H_2O (9:1, v/v) appeared at 498 nm. When Ag^{+} and Hg^{2+} were added, the absorption wavelength bathochromically shifted to 533 nm and 535 nm,

respectively, while addition of other metal ions (Li^+, Na^+, K^+, Cu^{2+}, Fe^{2+}, Zn^{2+}, Co^{2+}, Ni^{2+}, Mn^{2+}, Sr^{2+}, Ca^{2+}, Mg^{2+}, Al^{3+}, Cr^{3+} and Fe^{3+}) did not cause substantial change in the absorption spactrum, as showed in Fig. 4 (a). This means that probe **N-FP** is applicable for spectral detection of Ag^+ and Hg^{2+} from other common competitive metal ions.

By exciting at a wavelength of 498 nm, fluorescence emission spectra of probe **N-FP** (20 μM) before and after addition of equimolar different metal ions (Li^+, Na^+, K^+, Ag^+, Cu^{2+}, Fe^{2+}, Zn^{2+}, Co^{2+}, Ni^{2+}, Mn^{2+}, Sr^{2+}, Hg^{2+}, Ca^{2+}, Mg^{2+}, Al^{3+}, Cr^{3+} and Fe^{3+}) in EtOH/H_2O (9:1, v/v) were determined and showed in Fig. 4 (b). It was visible that the intensity of the fluorescence emission peak at 661 nm increased significantly after addition of Ag^+ and Hg^{2+}, while the fluorescence emission of probe **N-FP** remianed essentially unchanged upon addition of other common metal ions. So probe **N-FP** served fluorogenic chemosensor for detection of Ag^+ and Hg^{2+} and was useful for distinguishing Hg^{2+} from Ag^+ by UV-vis absorption spectral measurement.

Fig. 3. Color of probe **N-FP** solution in EtOH/H_2O (9:1, v/v) after addition of 1 equivalent of different metal ions (Li^+, Na^+, K^+, Ag^+, Cu^{2+}, Fe^{2+}, Zn^{2+}, Co^{2+}, Ni^{2+}, Mn^{2+}, Sr^{2+}, Hg^{2+}, Ca^{2+}, Mg^{2+}, Al^{3+}, Cr^{3+} and Fe^{3+}).

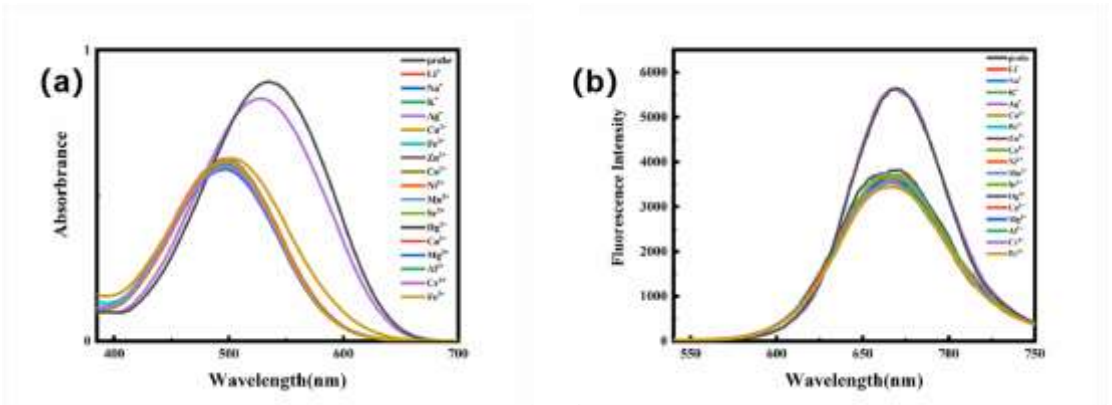

Fig. 4. UV-vis absorption (a) and fluorescence emission spectra (b) of probe **N-FP** (20 μM) before and after addition of equimolar different metal ions (Li^+, Na^+, K^+, Ag^+, Cu^{2+}, Fe^{2+}, Zn^{2+}, Co^{2+}, Ni^{2+}, Mn^{2+}, Sr^{2+}, Hg^{2+}, Ca^{2+}, Mg^{2+}, Al^{3+}, Cr^{3+} and Fe^{3+}) in EtOH/H_2O (9:1, v/v) with excitation wavelength of 498 nm.

*3.4 Anti-interference test on probe **N-FP** for detection of Ag^+ and Hg^{2+}*

In order to further verify whether probe **N-FP** had high selectivity for detection of Ag^+ and Hg^{2+} in the presence of common competitive metal ions, fluorescence emission intensities at 661 nm of probe **N-FP** (20 μM) after addition of different metal ions (20 μM) without (black bars) or with 20 μM of Hg^{2+} or Ag^+ ions (red bars) in EtOH/H_2O (9:1, v/v) were obtained and showed in Fig. 5. Addition of different metal ions (Li^+, Na^+, K^+, Cu^{2+}, Fe^{2+}, Zn^{2+}, Co^{2+}, Ni^{2+}, Mn^{2+}, Sr^{2+}, Ca^{2+}, Mg^{2+}, Al^{3+}, Cr^{3+} and Fe^{3+}) to the test solution containing probe **N-FP** and Ag^+ or Hg^{2+} (20 μM) did not cause substantial change in the fluorescence intensity at 661 nm. These test results demonstrated that other common metal ions had little effect on the selective detection of Ag^+ and Hg^{2+} by probe **N-FP** which showed high anti-interference ability for the fluorogenic sensing of Ag^+ and Hg^{2+}.

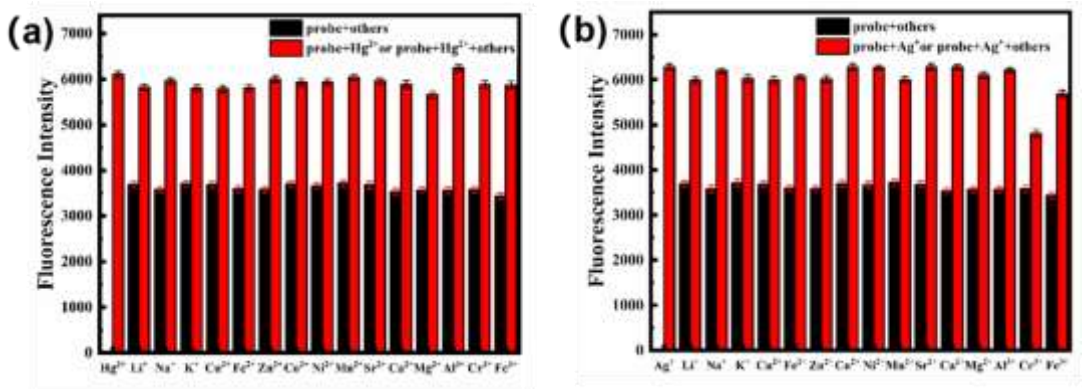

Fig. 5. Fluorescence emission intensities at 661 nm of probe **N-FP** (20 μM) upon addition of different metal ions (20 μM) without (black bars) or with 20 μM of Hg^{2+} ions (red bars) (a) or Ag^+ ions (red bars) (b) in EtOH/H_2O (9:1, v/v).

*3.5 Study on Ag^+ and Hg^{2+} detection limits by probe **N-FP***

In order to study the minimum detectable concentrations of Ag^+ and Hg^{2+} by probe **N-FP**, fluorescence spectra of probe **N-FP** containing different concentrations (2, 4, 6, 8, 10, 12, 14, 16, 18, 20 μM) of Ag^+ or Hg^{2+} were measured and showed in Fig. 6 (a) and (c), respectively. From the figures the relationahip between the fluorescence emission intensity at 661 nm and concentration of Ag^+ or Hg^{2+} was obtained as showed in Fig. 6 (b) and (d), respectively. The spectral results revealed that the fluorescence intensity at 661 nm of the solution increased with the increase of Ag^+ or Hg^{2+} concentration. The fluorescence intensity of the solution has a good linear

relationship with Ag^+ concentration and the linear correlation equation could be described as Y = 83.68182X + 2904.6, with the correlation coefficient R^2 = 0.99601. Similarly, the good linear relationship between the fluorescence intensity of the solution and Hg^{2+} could be described by the equation Y = 121.3X + 3853.4, with the correlation coefficient R^2 = 0.98275. According to the formula L = 3S/K, the minimum limit of detection (LOD) of probe **N-FP** for Ag^+ and Hg^{2+} ions was calculated to be 1.1 μM and 0.72 μM, respectively, where L is the detection limit, S is the standard deviation, and K denotes the slope of the fitting curve.

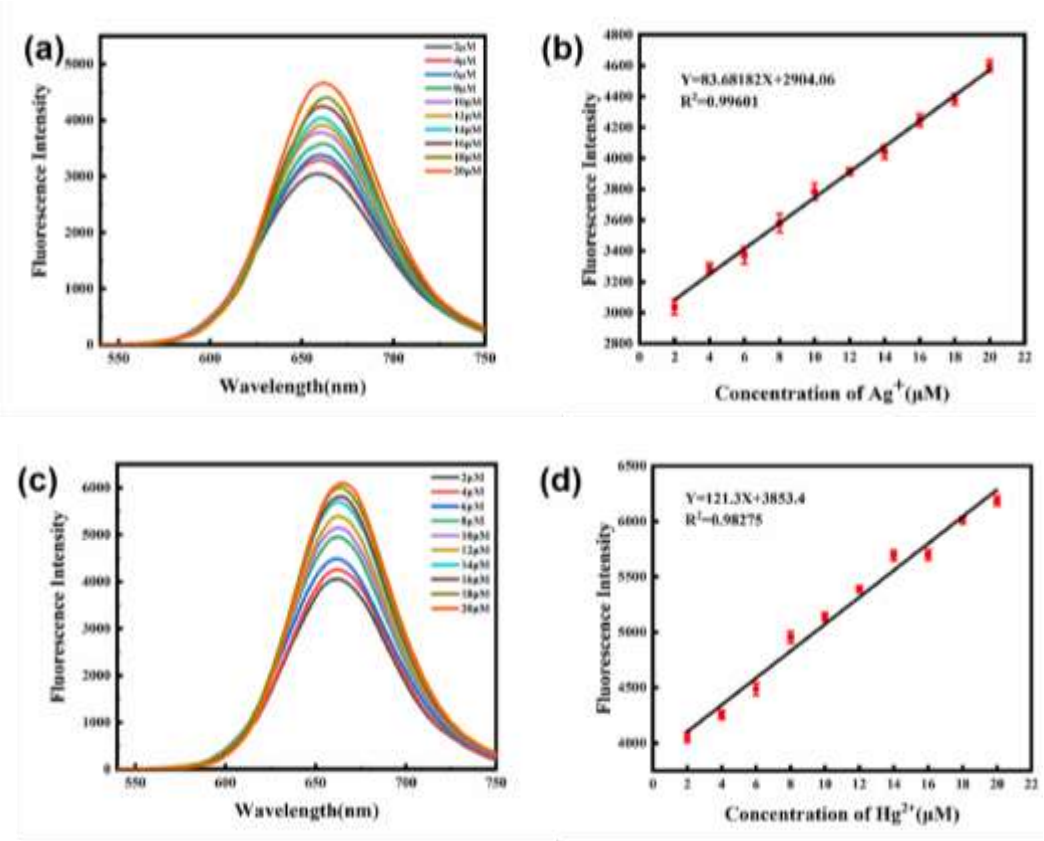

Fig. 6. Fluorescence spectra (a) and fluorescence emission intensities at 661 nm (b) of probe **N-FP** containing different concentrations of Ag^+ and fluorescence spectra (c) and fluorescence emission intensities at 661 nm (d) of probe **N-FP** containing different concentrations of Hg^{2+}.

*3.6 Study on the response time of probe **N-FP** to Ag^+ and Hg^{2+}*

In order to determine the sensitivity of probe **N-FP** for detection of Ag^+ and Hg^{2+}, fluorescence spectra of probe **N-FP** (λ_{ex} = 498 nm) at different time upon addition of Ag^+ or Hg^{2+} were measured. From the spectra changes in the fluorescence intensity at 661 nm of probe **N-FP** (20 μM) with time upon addition of 20 μM of Ag^+ or Hg^{2+}

ions in EtOH/H_2O (9:1, v/v) were obtained as showed in Fig. 7 (a) and (b). After Ag^+ was added, the fluorescence intensity of probe **N-FP** increased sharply within 3 min, then rose gradually until the fluorescence intensity reached equilibrium after 18 min. In the case of Hg^{2+}, the fluorescence intensity of probe **N-FP** increased sharply within 1 min upon Hg^{2+} addition, then the incease speed slowed down and the fluorescence intensity reached the maximum value in 4 min and remained constant over the test time. The results indicated that probe **N-FP** responded to Ag^+ and Hg^{2+} rapidy within 1-3 min.

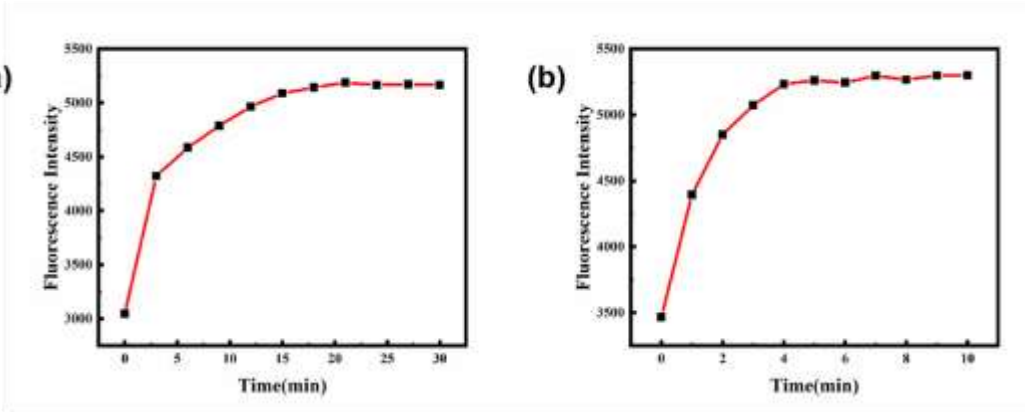

Fig. 7. Changes in the fluorescence intensity at 661 nm of probe **N-FP** (20 μM) with time (λ_{ex} = 498 nm) upon addition of 20 μM of Ag^+ (a) or Hg^{2+} ions (b) in EtOH/H_2O (9:1, v/v).

*3.7 Effect of pH on stability and applicability of probe **N-FP***

Probe **N-FP** solution (20 μM) in EtOH/H_2O (9/1, v/v) exhibited orange or reddish orange color at acidic, neutral, and alkaline conditions with pH less than 11. Distinct color change occurred under strongly alkaline conditions when pH value was 12-14, as showed in Fig. 8 (a). The results were in good accordance with the UV-vis absorption spectral measurement of probe **N-FP** (20 μM) at different pH, as showed in Fig. 8 (b). The maximum absorption wavelength at 498 nm of probe **N-FP** solution under acidic, neutral, and alkaline conditions with pH less than 11 shifted to 661 nm when pH was adjusted to 12-14. Fluorescence spectra of probe **N-FP** (20 μM) in EtOH/H_2O (9/1, v/v) at different pH were also determined and showed in Fig. 8 (c). It was observed that the fluorescence emission at 661 nm of probe **N-FP** solution under acidic, neutral, and alkaline conditions with pH less than 11 shifted to around 705 nm with significant decrease in the intensity when pH was 11-14. From the above results it could be concluded that the structure of probe **N-FP** was stable under acidic, neutral,

and weakly alkaline conditions, but transformed under strongly alkaline conditions. To investigate the applicable pH scale of probe **N-FP** for Hg^{2+}/Ag^{+} ions detection, fluorescence spectra of probe **N-FP** (20 μM) in EtOH/H_2O (9/1, v/v) at different pH after adding Hg^{2+} (20 μM) were measured and showed in Fig. 8 (d). It revealed that probe **N-FP** showed strong emission at 661 nm under acidic, neutral, and alkaline conditions with pH less than 11 after addition of Hg^{2+} while the emission shifted to about 705 nm accompanying remarkable decrease in the fluorescence intensity under pH 11-14, indicating that probe **N-FP** could be used for Hg^{2+} sensing under pH 1-10 conditions. In order to further reveal the structural transformation of probe **N-FP** under strongly alkaline conditions, LC-MS of probe **N-FP** after treatment with strong base was determined (Fig. S7), which displayed a signal of m/z 361 corresponding to the molecular ion peak of the hydrolyzed product of probe **N-FP**, as showed in Fig. 8 (e). These results indicated that probe **N-FP** readily hydrolyzed in the presence of strong base, consistent with the previous report [67].

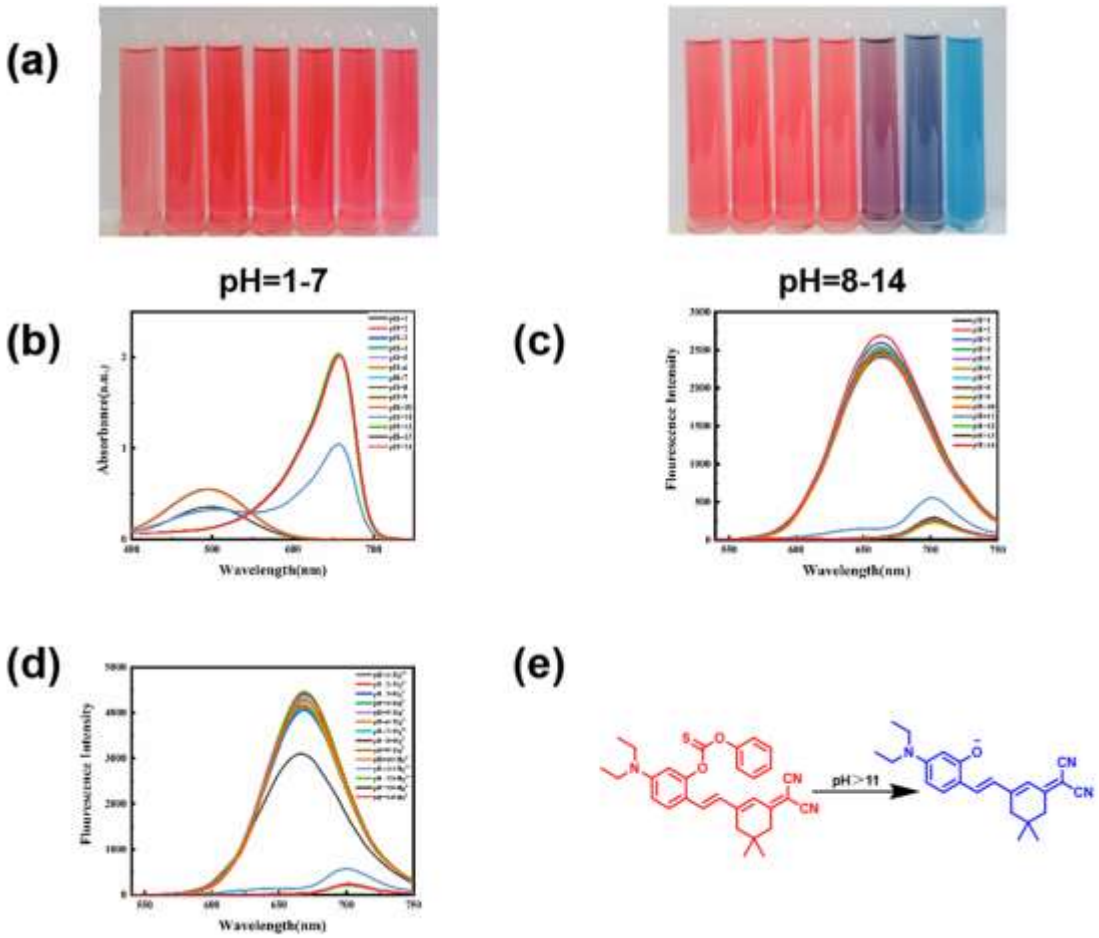

Fig. 8. (a) Color of probe **N-FP** solution (20 μM) in EtOH/H_2O (9/1, v/v) at different pH. UV-vis absorption (b) and fluorescence emission spectra (c) of probe **N-FP** (20 μM) at different pH. (d) Fluorescence spectra of probe **N-FP** (20 μM) in EtOH/H_2O

(9/1, v/v) at different pH after adding Hg^{2+} (20 μM). (e) Plausible structural change of probe **N-FP** (20 μM) in EtOH/H_2O (9/1, v/v) at strongly alkaline conditions (pH > 11).

*3.8 Comparison of sensing performance of probe **N-FP** with other Hg^{2+}/Ag^{+} sensors*

Comparison of the performance including excitation and emission wavelength, sensing mode, LOD, and applicable pH range of probe **N-FP** with other documented fluorescent probes for Hg^{2+} and Ag^{+} detection was summarized in Table 1. Among these fluorescent sensors for monitoring Hg^{2+} and Ag^{+}, some recognized Hg^{2+} and Ag^{+} through fluorescence turn-off mode [28,33,40], which was susceptible to interference from both background and coexisting competitive metal ions. Probe **L** and **RBSe** exhibited high sensitivity for Hg^{2+} and Ag^{+} sensing, but both could not be utilized under strongly acidic conditions [35,68]. From the table it was concluded that probe **N-FP** displayed the following advantages compared to other $Hg^{2+/}Ag^{+}$ fluorogenic sensors: (1) Selective detection of $Hg^{2+/}Ag^{+}$ by dual colorimetric and NIR fluorescence turn-on mode with a large Stokes shift of 163 nm; (2) Steady sensing of Hg^{2+} and Ag^{+} in a wide pH range; (3) Excellent adaptability even at extremely strong acid conditions.

Table 1

Comparison of performance of different fluorescent probes for $Hg^{2+/}Ag^{+}$ detection.

Probe	$\lambda_{ex}/\lambda_{em}$ (nm)	Fluorescence	Colorimetric	LOD for $Hg^{2+/}Ag^{+}$	Applicable pH	Ref.
Si NPs	370/450	turn-off	yes	2.676 μM/ 0.457 μM	> 7	[28]
3a	437/520	turn-off	yes	0.83 μM/ 1.20 μM	7–12	[33]
L	410/~530	turn-on	yes	20 nM/ 40 nM	6–10	[35]
D1	330/456	turn-off	yes	0.662 μM/ 19.9 μM	3.0	[40]
CL	379/695	turn-on	yes	0.83 μM/ 8.8 μM	2–12	[55]
NIFP	390/520	turn-on	yes	6.0 μM/ 0.48 μM	1–7	[64]
RBSe	520/580	turn-on	no	23 nM/	7.4	[68]

N-FP	498/661	turn-on	yes	52 nM 0.72 μM/ 1.1 μM	1–10	this work

*3.9 Study on the detection mechanism of probe **N-FP***

Possible detection mechanism of probe **N-FP** towards Hg^{2+} and Ag^{+} was showed in Fig. 9. Owing to the blocking of the intramolecular charge transfer (ICT) by the thiocarbonate moiety, probe **N-FP** exhibited weak fluorescence. When Ag^{+} or Hg^{2+} was added, it binded to sulfur due to its strong thiophilicity and triggered cleavage of C–O bond and elimination of Ag_2S or HgS to produce the intermediate **N-OH** which was strongly fluorescent due to recovery of ICT effect. Structure of the intermediate **N-OH** formed after addition of Ag^{+} or Hg^{2+} to probe **N-FP** was confirmed by ^{1}H NMR measurement. ^{1}H NMR spectrum of the product formed after addition of Ag^{+} to probe **N-FP** (Fig. S8) was essentially the same as that of compound **N-OH** [66]. Supports of the above proposed sensing mechanism by HPLC (Fig. S9 and Fig. S10) and LC-MS (Fig. S11 and Fig. S12) test were also confirmed.

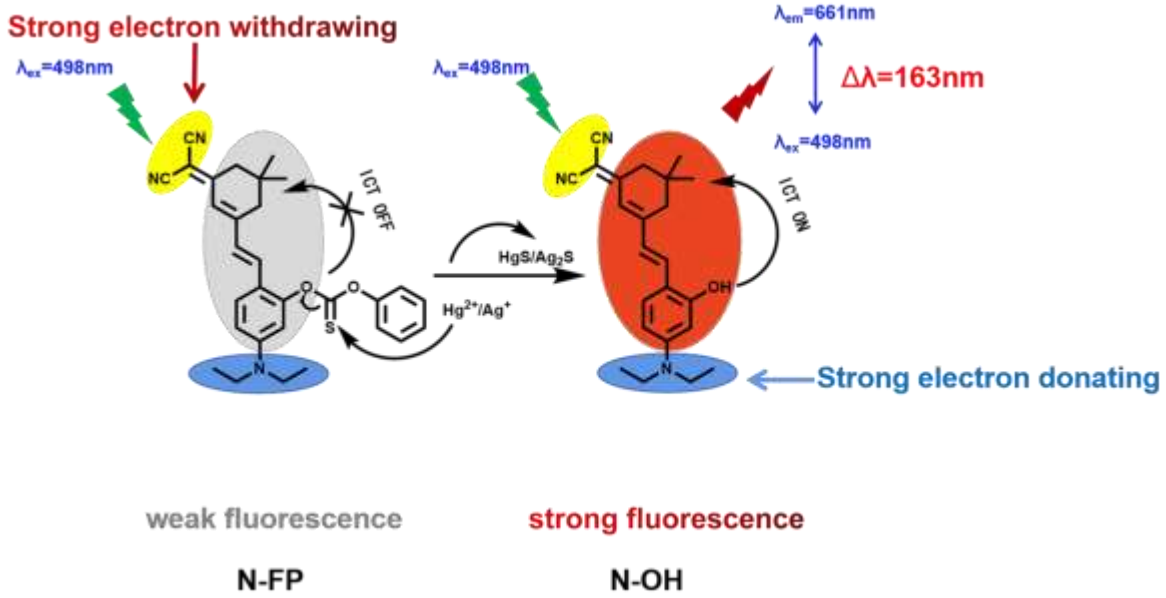

Fig. 9. Possible sensing mechanism of probe **N-FP** towards Hg^{2+} and Ag^{+}.

4. Conclusions

In summary, a new NIR fluorescent probe **N-FP** based on dicyanoisophorone was developed for selective detection of Ag^{+} and Hg^{2+}. The probe displayed a large Stokes shift of 163 nm and high stability in a broad pH range including strongly acidic conditions. When Ag^{+} or Hg^{2+} was added to probe **N-FP** solution in EtOH/H_2O (9:1, v/v), significant enhancement of fluorescence emission at 661 nm, bathochromic shift of UV-vis absorption wavelength, and color change from orange to red or purple were induced. Addition of other common metal ions including Li^{+}, Na^{+}, K^{+}, Ag^{+}, Cu^{2+}, Fe^{2+}, Zn^{2+}, Co^{2+}, Ni^{2+}, Mn^{2+}, Sr^{2+}, Ca^{2+}, Mg^{2+}, Al^{3+}, Cr^{3+} and Fe^{3+} failed to cause obvious change in the spectra and color. LOD of probe **N-FP** for Ag^{+} and Hg^{2+} was calculated to be 1.1 μM and 0.72 μM, respectively. Probe **N-FP** responded to Ag^{+} and Hg^{2+} quickly within 1-3 min and could be utilized for sensing Ag^{+} and Hg^{2+} in a pH range of 1-10. ^{1}H NMR, HPLC and MS measurements revealed that the sensing mechanism was based on Ag^{+}/Hg^{2+}-induced hydrolysis of probe **N-FP** which led to recovery of ICT and fluorescence enhancement.

Acknowledgements

The Funding for the Open Research Program of State Key Laboratory of Molecular Engineering of Polymers, Fudan University (K2022-38 to Yanxi Song) is acknowledged.

ORCID

Hongqi Li https://orcid.org/0000-0002-8648-3634.

REFERENCES

1. Valko MM, Morris H, Crinin MT. Metals, toxicity and oxidative stress. *Curr Med Chem*. 2005;12:1161–1208.
2. Coelho Junior GS, Fontana KB, Maranhão TA, Borges DLG. Dielectric barrier discharge-assisted determination of methylmercury in particulate matter by atomic absorption spectrometry. *Anal Methods*. 2022;14:1371–1377.

3. Thulasidas SK, Kulkami MJ, Porwal NK, Page AG, Sastry MD. Direct determination of beryllium, cadmium, lithium, lead and silver in thorium nitrate solution by electrothermal atomization atomic absorption spectrometry. *Anal Lett*. 1998;21:265–278.
4. Tutschku S, Schantz MM, Wise S. Determination of methylmercury and butyltin compounds in marine biota and sediments using microwave-assisted acid extraction, solid-phase microextraction, and gas chromatography with microwave-induced plasma atomic emission spectrometric detection. *Anal Chem*. 2002;74:4694–4701.
5. Da Silva MJ, Paim AP, Pimentel MF, Cervera ML, De la Guardia M. Determination of mercury in rice by cold vapor atomic fluorescence spectrometry after microwave-assisted digestion. *Anal Chim Acta*. 2010;667:43–48.
6. Wang Y, Zhang L, Han X, Zhang L, Wang X, Chen L. Fluorescent probe for mercury ion imaging analysis: strategies and applications. *Chem Eng J*. 2021;406:127166.
7. Samanta T, Shunmugam R. Colorimetric and fluorometric probes for the optical detection of environmental Hg(II) and As(III) ions. *Mater Adv*. 2021;2:64–95.
8. Chen S-Y, Li Z, Li K, Yu X-Q. Small molecular fluorescent probes for the detection of lead, cadmium and mercury ions. *Coord Chem Rev*. 2021;429:213691.
9. AbhijinaKrishna R, Velmathi S. A review on fluorimetric and colorimetric detection of metal ions by chemodosimetric approach 2013-2021. *Coord Chem Rev*. 2022;459:214401.
10. González-González RB, Morales-Murillo MB, Martínez-Prado MA, Melchor-Martínez FM, Ahmed I, Bilal M, Parra-Saldívar R, Iqbal HMN. Carbon dots-based nanomaterials for fluorescent sensing of toxic elements in environmental samples: strategies for enhanced performance. *Chemosphere*. 2022;300:134515.
11. Ayodhya D. A review on recent advances in selective and sensitive detection of heavy toxic metal ions in water using g-C_3N_4-based heterostructured composites. *Mater Chem Front*. 2022;6:2610–2650.
12. Xu D, Jia H, Niu Y, Yin S. Fluorine-boron compound-based fluorescent chemosensors for heavy metal ion detection. *Dyes Pigm*. 2022;200:110185.

13. Raveendran AV, Sankeerthana PA, Jayaraj A, Swamy PCA. Recent developments on BODIPY based chemosensors for the detection of group IIB metal ions. *Results Chem*. 2022;4:100297.
14. Huang NH, Liu Y, Li RT, Chen J, Hu PP, Young DJ, Chen JX, Zhang WH. Sequential Ag^{+}/biothiol and synchronous Ag^{+}/Hg^{2+} biosensing with zwitterionic Cu^{2+}-based metal-organic frameworks. *Analyst*. 2020;145:2779– 2788.
15. Pavadai R, Amalraj A, Subramanian S, Perumal P. High catalytic activity of fluorophore-labeled Y-shaped DNAzyme/3D MOF-MoS_2NBs as a versatile biosensing platform for the simultaneous detection of Hg^{2+}, Ni^{2+}, and Ag^{+} ions. *ACS Appl Mater Interfaces*. 2021;13:31710–31724.
16. Pavadai R, Perumal P. An innovative trimetallic-MOF mediated catalytic cleavage activity of FAM tagged Ag10/T-rich DNAzyme as an ultra-sensitive and selective fluorescent biosensor for subsequent recognition of Ag^{+} and Hg^{2+} ions. *J Photochem Photobiol A*. 2022;429:113901.
17. Balamurugan A, Lee H-i. Aldoxime-derived water-soluble polymer for the multiple analyte sensing: consecutive and selective detection of Hg^{2+}, Ag^{+}, ClO^{-}, and cysteine in aqueous media. *Macromolecules*. 2015;48:3934–3940.
18. Wei G, Jiang Y, Wang F. A novel AIEE polymer sensor for detection of Hg^{2+} and Ag^{+} in aqueous solution. *J Photochem Photobiol A*. 2018;358:38–43.
19. Xiao L, Sun Q, Zhao Q, Cheng X. Highly sensitive and selective fluorescent monomer/polymer probes for Hg^{2+} and Ag^{+} recognition and imaging of Hg^{2+} in living cells. *Anal Bioanal Chem*. 2020;412:881–894.
20. Lin Z, Li X, Kraatz HB. Impedimetric immobilized DNA-based sensor for simultaneous detection of Pb^{2+}, Ag^{+}, and Hg^{2+}. *Anal Chem*. 2011;83:6896– 6901.
21. He X, Qing Z, Wang K, Zou Z, Shi H, Huang J. Engineering a unimolecular multifunctional DNA probe for analysis of Hg^{2+} and Ag^{+}. *Anal Methods*. 2012;4:345–347.
22. Wu Z, Feng M, Chen X, Tang X. N-dots as a photoluminescent probe for the rapid and selective detection of Hg^{2+} and Ag^{+} in aqueous solution. *J Mater Chem B*. 2016;4:2086–2089.
23. Pashazadeh-Panahi P, Hasanzadeh M, Eivazzadeh-Keihan R. A novel optical probe based on D-penicillamine-functionalized graphene quantum dots: preparation and application as signal amplication element to minoring of ions in human biofluid. *J Mol Recognit*. 2020;33:e2828.

24. He Y, Wang Y, Mao G, Liang C, Fan M. Ratiometric fluorescent nanoprobes based on carbon dots and multicolor CdTe quantum dots for multiplexed determination of heavy metal ions. *Anal Chim Acta*. 2022;1191:339251.
25. Ren G, Zhang Q, Li S, Fu S, Chai F, Wang C, Qu F. One pot synthesis of highly fluorescent N doped C-dots and used as fluorescent probe detection for Hg^{2+} and Ag^{+} in aqueous solution. *Sens Actuators B*. 2017;243:244–253.
26. Zhang Y, Jiang H, Wang X. Cytidine-stabilized gold nanocluster as a fluorescence turn-on and turn-off probe for dual functional detection of Ag^{+} and Hg^{2+}. *Anal Chim Acta*. 2015;870:1–7.
27. Duan B, Wang M, Li Y, Jiang S, Liu Y, Huang Z. Dual-emitting zein-protected gold nanoclusters for ratiometric fluorescence detection of Hg^{2+}/Ag^{+} ions in both aqueous solution and self-assembled protein film. *New J Chem*. 2019;43:14678–14683.
28. Zhu B, Ren G, Tang M, Chai F, Qu F, Wang C, Su Z. Fluorescent silicon nanoparticles for sensing Hg^{2+} and Ag^{+} as well visualization of latent fingerprints. *Dyes Pigm*. 2018;149:686–695.
29. Chu Z-Y, Wang W-N, Zhang C-Y, Ruan J, Chen B-J, Xu H-M, Qian H-S. Monitoring and removal of trace heavy metal ions via fluorescence resonance energy transfer mechanism: in case of silver ions. *Chem Eng J*. 2019;375:121927.
30. Wang ZX, Ding SN. One-pot green synthesis of high quantum yield oxygen-doped, nitrogen-rich, photoluminescent polymer carbon nanoribbons as an effective fluorescent sensing platform for sensitive and selective detection of silver(I) and mercury(II) ions. *Anal Chem*. 2014;86:7436–7445.
31. Xiao L, Liu K, Duan L, Cheng X. Reaction-based fluorescent silk probes with high sensitivity and selectivity to Hg^{2+} and Ag^{+} ions. *J Mater Chem C*. 2021;9:4877–4887.
32. Khoshbin Z, Housaindokht MR, Verdian A. A low-cost paper-based aptasensor for simultaneous trace-level monitoring of mercury (II) and silver (I) ions. *Anal Biochem*. 2020;597:113689.
33. Ye F, Liang XM, Pang XX, Xu KX, Chai Q, Fu Y. A novel dithiourea-appended naphthalimide "on-off" fluorescent probe for detecting Hg^{2+} and Ag^{+} and its application in cell imaging. *Talanta*. 2019;200:494–502.

34. Bahta M, Ahmed N. An AIEE active 1,8-naphthalimide-sulfamethizole probe for ratiometric fluorescent detection of Hg^{2+} ions in aqueous media. *J Photochem Photobiol A*. 2020;391:112354.
35. Mahata S, Kumar S, Dey S, Mandal BB, Manivannan V. A probe with hydrazinecarbothioamide and 1,8-naphthalimide groups for "turn-on" fluorescence detection of Hg^{2+} and Ag^{+} ions and live-cell imaging studies. *Inorg Chim Acta*. 2022;535:120876.
36. Chen YJ, Chen MY, Lee KT, Shen LC, Hung HC, Niu HC, Chung WS. 1,3-Alternate calix[4]arene functionalized with pyrazole and triazole ligands as a highly selective fluorescent sensor for Hg^{2+} and Ag^{+} ions. *Front Chem*. 2020;8:593261.
37. Rodriguez-Lavado J, Lorente A, Flores E, Ochoa A, Godoy F, Jaque P, Saitz C. Elucidating sensing mechanisms of a pyrene excimer-based calix[4]arene for ratiometric detection of Hg^{2+} and Ag^{+} and chemosensor behaviour as INHIBITION or IMPLICATION logic gates. *RSC Adv*. 2020;10:21963–21973.
38. Saiyasombat W, Kiatisevi S. Bis-BODIPY linked-triazole based on catechol core for selective dual detection of Ag^{+} and Hg^{2+}. *RSC Adv*. 2021;11:3703– 3712.
39. Nie K, Dong B, Shi H, Liu Z, Liang B. Thienyldiketopyrrolopyrrole as a robust sensing platform for multiple ions and its application in molecular logic system. *Sens Actuators B*. 2017;244:849–853.
40. Chen Z-E, Zhang H, Iqbal Z. A new thiosemicarbazone fluorescent probe based on 9,9'-anthracece for Hg^{2+} and Ag^{+}. *Spectrochim Acta A*. 019;215:34–40.
41. Wu Y-T, Zhao J-L, Mu L, Zeng X, Wei G, Redshaw C, Jin Z. A 2-Styryl-1,8-naphthyridine derivative as a versatile fluorescent probe for the selective recognition of Hg^{2+}, Ag^{+} and F^{-} ions by tuning the solvent. *Sens Actuators B*. 2017;252:1089–1097.
42. Lee SY, Bok KH, Kim C. A fluorescent "turn-on" chemosensor for Hg^{2+} and Ag^{+} based on NBD (7-nitrobenzo-2-oxa-1,3-diazolyl). *RSC Adv*. 2017;7:290–299.
43. Shi W, Sun S, Li X, Ma H. Imaging different interactions of mercury and silver with live cells by a designed fluorescence probe rhodamine B selenolactone. *Inorg Chem*. 2010;49:1206–1210.
44. Shen W, Wang L, Wu M, Bao X. A fluorescein derivative FLTC as a chemosensor for Hg^{2+} and Ag^{+} and its application in living-cell imaging. *Inorg Chem Commun*. 2016;70:107–110.

45. Tsukamoto K, Shinohara Y, Iwasaki S, Maeda H. A coumarin-based fluorescent probe for Hg^{2+} and Ag^{+} with an N'-acetylthioureido group as a fluorescence switch. *Chem Commun*. 2011;47:5073–5075.

46. Thamaraiselvi P, Duraipandy N, Kiran MS, Easwaramoorthi S. Triarylamine rhodanine derivatives as red emissive sensor for discriminative detection of Ag^{+} and Hg^{2+} ions in buffer-free aqueous solutions. *ACS Sustainable Chem Eng*. 2019;7:9865–9874.

47. Qu W-J, Fang H, An J-N, Yang H-H, He J-X, Yao H, Wei T-B, Lin Q, Zhang Y-M. Highly sensitive detection of mercury(II) and silver(I) ions in aqueous solution via a chromene-functionalized imidazophenazine derivative. *J Photochem Photobiol A*. 2020;402:112814.

48. Raza R, Dey N, Panja A, Ghosh K. Pyridyl azo-based progelator in selective sensing of Hg^{2+} and Ag^{+} ions via sol to gel conversion. *ChemistrySelect*. 2019;4:11564–11571.

49. Chen J, Wang N, Tong H, Song C, Ma H, Zhang Y, Gao F, Xu H, Wang W, Lou K. A compact fluorescence/circular dichroism dual-modality probe for detection, differentiation, and detoxification of multiple heavy metal ions via bond-cleavage cascade reactions. *Chin Chem Lett*. 2021;32:3876–3881.

50. Zeng J, Hua X-W, Bao Y-W, Wu F-G. Orange-emissive sulfur-doped organosilica nanodots for metal ion/glutathione detection and normal/cancer cell identification. *ACS Appl Nano Mater*. 2021;4:6083–6092.

51. Lu Z, Wang P, Xiong W, Qi B, Shi R, Xiang D, Zhai K. Simultaneous detection of mercury (II), lead (II) and silver (I) based on fluorescently labelled aptamer probes and graphene oxide. *Environ Technol*. 2021;42:3065–3072.

52 Chandrasekaran PO, Aswathy A, James K, Kala K, Ragi MT, Manoj N. A molecular chameleon: fluorometric to Pb^{2+}, fluorescent ratiometric to Hg^{2+} and colorimetric to Ag^{+} ions. *J Photochem Photobiol A*. 2021;407:113050.

53. Krishnaveni K, Iniya M, Siva A, Vidhyalakshmi N, Sasikumar S, Ramesh UKP, Murugesan S. Naphthyl hydrazone anchored with nitrosalicyl moiety as fluorogenic and chromogenic receptor for heavy metals (Ag^{+}, Hg^{2+}) and biologically important F^{-} ion and its live cell imaging applications in HeLa cells and zebrafish embryos. *J Mol Struct*. 2020;1217:128446.

54. Darroudi M, Ziarani GM, Ghasemi JB, Badiei A. Facile and green preparation of colorimetric and fluorescent sensors for mercury, silver, and carbonate ions

visual detecting: spectroscopy and theoretical studies. *J Mol Struct*. 2021;1241:130626.

55. Jiang L, Zheng T, Xu Z, Li J, Li H, Tang J, Liu S, Wang Y. New NIR spectroscopic probe with a large Stokes shift for Hg^{2+} and Ag^{+} detection and living cells imaging. *Spectrochim Acta A*. 2022;271:120916.
56. Li Y, Zhou Y, Lei J, Lu Q, Qin X, Xu Q, Wang Y, Wu C, Yang Z, He B. A NIR fluorescent probe for the selective detection of hydrogen peroxide by acetyl-hydrolyzing in cells. *J Mol Struct*. 0223;1271:134042.
57. Yuan D, Pan K, Xu S, Wang L. Dual channel recognition of human serum albumin and glutathione by fluorescent probes with site-dependent responsive features. *Anal Chem*. 2022;94:12391–12397.
58. Qin J, Tian H, Kong F, Guo Y, Du W, Zhang C, Gu H, Li Y. Construction of GSH activated near-infrared fluorescent and photoacoustic dual-modal probe for in vivo tumor imaging. *Sens Actuators B*. 2022;371:132522.
59. Yue L, Huang H, Song W, Lin W. A near-infrared endoplasmic reticulum-targeted fluorescent probe to visualize the fluctuation of SO_2 during endoplasmic reticulum stress. *Chem Eng J*. 202;431:133468.
60. Chen Z, Wang B, Liang Y, Shi L, Cen X, Zheng L, Liang E, Huang L, Cheng K. Near-infrared fluorescent and photoacoustic dual-mode probe for highly sensitive and selective imaging of cysteine in vivo. *Anal Chem*. 2022;94:10737–10744.
61. Yang Q, Xie C, Luo K, Tan L, Peng L, Zhou L. Rational construction of a new water soluble turn-on colorimetric and NIR fluorescent sensor for high selective Sec detection in Se-enriched foods and biosystems. *Food Chem*. 2022;394:133474.
62. Ni J-Y, Zhang X-Q, Wang M-Y, Yu Q, Su R, Xu Y-J, Song Y-L, Ge J-F. Dicyanoisophorone derivatives with self-targeting abilities towards multiple organelles for fluorescent markers and viscosity detection. *Sens Actuators B*. 2022;367:132065.
63. Wang Y, Niu H, Wang K, Wang G, Liu J, James TD, Zhang H. mtDNA-specific ultrasensitive near-infrared fluorescent probe enables the differentiation of healthy and apoptotic cells. *Anal Chem*. 2022;94:7510–7519.
64. Qi Y, Li Y, Nan T, Li H, Tang J, Liu S, Wang Y. A novel fluorescent probe with large Stokes shift for the detection of Ag^{+} and Hg^{2+}. *Opt Mater*. 2022;123:111929.

65. Hu Q, Huang Q, Mao Y, Liu X, Tan F, Wang Y, Yin Q, Wu X, Wang H. A near-infrared large Stokes shift probe based enhanced ICT strategy for F^- detection in real samples and cell imaging. *Tetrahedron*. 2019;75:130762.
66. Zhang Y, Hao Y, Ma X, Chen S, Xu M. A dicyanoisophorone-based highly sensitive and selective near-infrared fluorescent probe for sensing thiophenol in water samples and living cells. *Environ Pollut*. 2020;265:114958.
67. Xue T, Dai Y, Zhang X, Cheng Y, Gu X, Ji H, Misal S, Qi Z. Ultrasensitive near-infrared fluorescent probe with large stokes shift for real-time tracing of CYP1A1 in living cells and zebrafish model. *Sens Actuators B*. 2019;293:265–272.
68. Shi W, Sun S, Li X, Ma H. Imaging different interactions of mercury and silver with live cells by a designed fluorescence probe rhodamine B selenolactone. *Inorg Chem*. 2010;49:1206–1210.